Revealing the factors influencing grain boundary segregation of P, As in Si: Insights from first-principles

Dongdong Zhao, Yanjun Li*

Department of Materials Science and Engineering, Norwegian University of Science and Technology (NTNU), 7491 Trondheim, Norway

*Corresponding author. E-mail: yanjun.li@ntnu.no Tel.: +47 73551206

Abstract

Phosphorous (P) and arsenic (As) segregation at grain boundaries (GBs) usually deteriorate the electrical performance of *n*-type doped Si-wafers. In order to probe the factors influencing P and As segregation behaviors along Si GBs, a systematic investigation upon the interactions between P, As atoms and a series of coincidence site lattice Si GBs, including Σ3 {111}, Σ9 {221}, Σ27 {552}, Σ3 {112}, was carried out via first-principles calculations. It is revealed that the segregation behaviors of P, As along different GBs are different, which is dependent on both GB characteristics, i.e. the intrinsic lattice distortion, number of dangling/extra bonds, deep levels in the bandgap of density of states, and also the impurity properties. It reveals that smaller P atoms tend to segregate to the compressed atomic sites in GBs, by which the intrinsic GB lattice distortion is reduced. However, GB lattice distortion hardly induce As segregation owing to the similar atomic size between As and Si atoms. Calculations also indicate that under-coordinated core sites with dangling bond along GBs are remarkably attractive for P and As segregation, as a result of the nature of group-V elements to be three-coordinated rather than four-coordinated. Furthermore, GBs having deep levels in the bandgap of density of states, produced either by dangling or extra bonds, show a strikingly high attractive strength for both P and As segregation. The present work is supposed to provide important insights on substitutional impurity segregation along GBs in multi-crystalline Si in the atomic and electronic level.

Keywords: P/As segregation, coincidence site lattice (CSL), grain boundaries, multi-crystalline Si, first-principles calculations.

1. Introduction

Attractive impurity-grain boundary (GB) interactions generally induce impurity segregations at GBs, which would exert significant influence on GB properties and thereby pronouncedly affect the macroscopic properties of materials [1-4]. The modulation of material properties through microscopic manipulation of GB properties in terms of segregation engineering does not only work for metallic systems [5-7], but also for semiconductors, e.g. Si-based materials [8-12]. The alien elemental doping plays an important role in modulating the electrical properties of Si-based nano-devices [13-16]. A controlled doping of semiconductors forms the basis of photovoltaics, microelectronics, sensors, thermoelectric devices, and field effect transistors [16-19]. Phosphorous (P) and arsenic (As), as important *n*-type dopants, are usually ion implanted in Si wafers for nano-scale semiconductor applications [20-24]. One typical example is the metal-oxide semiconductor field effect transistor (MOSFET) [12, 19, 25]. The uniformity of doping elements is important for the electrical parameters of these Si-based microelectronic devices [25, 26]. Nevertheless, GB segregation usually occurs in the process of post-implant annealing, resulting in an non-uniform distribution of dopants [12, 27]. This dopant concentration difference at GB and grain interior is especially unwanted since it can induce characteristic electrical variability and drastically change the threshold voltage of MOSFET [11, 25, 28, 29]. Furthermore, dopant redistribution, produced by substantial GB segregation, also decreases the active dopant content in the grains, and hence reduces the overall conductivity of nano-devices [26]. As the feature size of transistors is scaling down over the past decades, the “intrinsic” variation in these transistor parameters due to this dopant concentration difference becomes increasingly pronounced since a localized dopant fluctuation is increasingly affecting the electrical characteristics of devices [24]. Consequently, the development of advanced nano-scale devices is calling for a more uniform distribution of implanted dopants, which would need an in-depth fundamental understanding of the segregation behavior of P and As along GBs in multi-crystalline Si (mc-Si).

Numerous experimental works have been conducted to investigate the segregation behavior of P and As along Si GBs by using different techniques including atom probe tomography (APT) [11, 12, 25, 26, 28], secondary ion mass spectroscopy (SIMS) [12, 26, 30], auger electron spectroscopy (AES)

[31], scanning transmission electron microscopy (STEM) [27, 32], etc. For instance, Inoue et al. [11, 28] using APT measurement, have mapped out the three dimensional P and As segregations at Si GBs in a *n*-type MOSFET. On basis of the experimental work, subsequent equilibrium (e.g. McLean isotherm) [26, 27, 33] and kinetic segregation [34] models have also been developed to depict the segregation behaviors of P and As along Si GBs. The segregation of P and As along Si GBs was ascribed to the fast dopant diffusion at GBs, slower dopant diffusion in grains, and recrystallization [11]. However, despite of these pioneering experimental and modelling works, the cause and underlying physics of P and As segregations at Si GBs are still less understood.

As a matter of fact, the dopant segregation profile along the GBs is determined by the dopant-GB interaction energy, which is also termed by *segregation energy*, i.e. the energy difference between the states of dopant atom at GB and in bulk lattice [35, 36]. The experimental *segregation energy* of P and As along Si GBs covers a range of 0.30-0.56 eV and 0.28-0.65 eV [26, 27, 32, 33, 37], respectively, most of which are acquired through fitting the experimental data via McLean isotherm. Nevertheless, macroscopic McLean isotherm is incapable of determining the specific energetically favorable sites along the GBs for P or As segregation. Fortunately, the rapid development of first-principles calculation approach in the last decades has made it possible to achieve quantitative understanding on the dopant-GB interactions, in terms of specific atomic sites, as well as *segregation energy* [38, 39]. Successful pioneering works have been contributed by Chisholm et al. [40] and Maiti et al. [41]. Using *ab initio* calculations, they have determined the segregation energy of As impurities along defect-free Σ5 {310} and Σ13 {150} GBs in Si in terms of isolated As atoms, dimers and chains, the value of which can be negative to -0.52 eV/atom. However, the specific interactions between P or As and other Si GBs remain largely unclear. A systematic investigation is thus required to address the P or As segregation behavior along Si GBs in a clearer manner. Such a work will enhance our understanding of dopant-GB interactions in mc-Si and therefore benefit the development of advanced mc-Si based nano-scale devices.

In this work, a systematic research, on basis of first-principles calculations, is undertaken to investigate the segregation behavior of P and As along Si GBs. The Σ3 {111}, Σ9 {221}, Σ27 {552},

Σ3 {112} GBs were selected as the representative Si GBs to interpret the dopant-GB interactions. It is worth noting that the Σ3 {111}, Σ9 {221}, Σ27 {552} GB, also termed as the first-, second-, third-order twin boundaries [42, 43], are the most frequently observed GBs in mc-Si, which can usually account for over 50% of the total GB population [44, 45]. The preferential segregation sites and corresponding *segregation energy* for P and As at these Si GBs were determined. Following that, the underlying physics and driving force of P and As segregations at Si GBs are discussed.

2. Grain boundary construction and calculation methodology

Exchange correlation functions treated with generalized gradient approximation (GGA) [46, 47] in the Perdew–Burke–Ernzerhof form [48], which is implemented in Vienna ab initio simulation package (VASP) [49, 50], were adopted to carry out the density functional theory (DFT) calculations in the present work. The energy cutoff was set to 400 eV. *k*-points sampling within the Monk-horst Pack scheme [51] was used for the integration of Brillouin-zone. Hellmann-Feynman force on all atoms being $< 10^{-2}$ eV·Å^{-1} was adopted for the termination of structural relaxations. Total energy calculations were performed using the linear tetrahedron method with Blöchl corrections [52].

To gain insight of the segregation behavior of P and As along Si GBs, bi-crystal supercells (cf. Fig. 1a) containing Σ3 {111}, Σ9 {221}, Σ27 {552}, Σ3 {112} GBs were created according to the experimental observations [53-55] and theoretical predictions [56-59]. One can find in Fig. 1a that each bi-crystal has two GBs and two micro-grains separated by the GBs. Fig. 1b-f shows the relaxed ground state structure of each GB, wherein the distinct core atomic sites for potential segregation of P and As atoms in each GB are labelled with numbers. Straight and zig-zag Σ3 {112} GBs (S-Σ3 {112} GB and A-Σ3 {112} GB) are both included for the sake of investigating the structure reconstruction effect on the P and As segregation along Si GBs. It is worth noting that both the S-Σ3 {112} GB and A-Σ3 {112} GB have two variants, i.e. (1×1) and (1×2) models [60], with the latter allowing for bonds reconstruction along the $< 1\bar{1}0 >$ direction and thus eliminating dangling bonds. Convergence test shows that the supercell size of each GB is sufficiently large to produce well converged results.

The GB energy, γ_{GB} of the Si GBs as investigated in the present work was calculated based on

[35]:

$$\gamma_{GB} = \left(E_{SiGB}^{tot} - N_{Si} E_{Si} \right) / 2A \quad (1)$$

Wherein, E_{SiGB}^{tot} is the calculated total DFT energy of the bi-crystal supercell shown in Fig. 1(a). N_{Si} is the number of atoms in each GB supercell, and E_{Si} is the reference energy of per Si atom, taken from the *diamond* phase. *A* is the GB cross-section area. The scaling factor ½ in Eq. (1) denotes the presence of two GBs in the bi-crystal supercell.

To explore the interactions between P, As solutes and GBs, the segregation energy of impurities at the GBs, γ_{seg}, was calculated in terms of

$$\gamma_{seg} = E_{ie}^{GB} - E_{ie}^{Bulk} \quad (2)$$

Wherein, E_{ie}^{GB} and E_{ie}^{Bulk} are the impurity energy of P or As atoms in a GB and bulk, respectively, which can be calculated using the following equations

$$E_{ie}^{GB} = E_{GB}^{Si_{n-1}X_1} - E_{GB}^{Si_{n-1}} - \mu_X \,,\ X = P, As \quad (3)$$

$$E_{ie}^{Bulk} = E_{Bulk}^{Si_{n-1}X_1} - E_{Bulk}^{Si_{n-1}} - \mu_X \,,\ X = P, As \quad (4)$$

Herein, $E_{GB}^{Si_{n-1}X_1}$ is the total energy of GB containing one impurity atom, $E_{GB}^{Si_{n-1}}$ represents the total energy of pure GB without alien impurities, while $E_{Bulk}^{Si_{n-1}X_1}$, $E_{Bulk}^{Si_{n-1}}$ for pure Si bulk with and without P or As impurity, respectively. μ_X is the chemical potential of per P or As atom, the value of which is taken from the orthorhombic phase [61, 62]. A negative value of γ_{seg} implies that the segregation of P or As impurity elements at Si GBs is energetically favorable.

3. Results

The properties of the GBs as investigated in the present work are summarized in Table 1, in which some previous theoretical data [35, 63] are also included for comparison. Apparently, Σ3 {111}

GB has the lowest γ_{GB} among all the GBs. One can also find that the (1×2) models of S- and A-Σ3 {112} GBs have smaller γ_{GB} than the corresponding (1×1) models. This is not surprising since in (1×2) models dangling bonds are eliminated as a result of reconstruction, which leads to the reduction of total DFT energy. Such an elimination of dangling bonds will not occur in the (1×1) models because of the periodicity of the supercell, where three coordinated atomic sites (e.g. site 1 in S-Σ3 {112} GB and sites 2, 9 in A-Σ3 {112} GB) are retained.

In the present work, more than 140 substitutional sites alongside the target GBs were calculated to check whether they were energetically favorable for P and As segregation. In addition, the interstitial segregation of P and As atoms towards the GBs was also investigated, with no energetically favorable sites having been identified. Here we will mainly focus on the segregation behavior of P and As as substitutional atoms along Si GBs.

3.1 Σ3 {111} GB

The γ_{seg} profile of P and As segregations at different GBs are displayed in Fig. 2a-b. As shown in Fig. 1b, Σ3 {111} GB has two core sites for possible As and P segregation. However, the slightly positive γ_{seg} indicates Σ3 {111} has no energetically favorable sites for the segregation of P and As atoms. The unfavorable segregation of P along Σ3 {111} GB predicted in this work is consistent with the experimental results based on APT analysis [64]: Σ3 {111} GB is intrinsically not able to getter P atoms even when the impurity concentration is high. Also, no As segregation along Σ3 {111} GBs has been observed, as reported in the experiments by Grovenor et al. [27], which is in agreement with our present predictions.

3.2 Σ9 {221} GB

A negative γ_{seg} was predicted for three sites (2, 4, 5) among the 8 core sites in Σ9 {221} GB for P segregation, indicating an attractive interaction between P and Σ9 {221} GB (cf. Fig. 2b). The other core sites are repulsive for P segregation. Site 5 has the most negative γ_{seg}, i.e. -0.189 eV/atom. This implies that Σ9 {221} GB is capable of gettering P atoms. The non-uniform γ_{seg} for different core sites

suggests that the P segregation towards Σ9 {221} GB is site-specific and heterogeneous. On the contrary, all core sites in the GB show positive γ_{seg} for As segregation (cf. Fig. 2b) indicating that the Σ9 {221} GB is energetically unfavorable for As segregation.

3.3 Σ27 {552} GB

As indicated in the calculated segregation profile of P along Σ27 {552} GB shown in Fig. 2a, the impurity-GB interaction was also atomic site dependent, wherein 9 core sites in Σ27 {552} GB are energetically favorable for P segregation, with site 12 (cf. Fig. 1f) having the most negative γ_{seg}, i.e. -0.4 eV/atom. As a symmetric site to site 12, site 12′ is calculated to possess the same value of γ_{seg} for P segregation. Moreover, one can find that core sites connecting one 7-membered and two 6-membered rings (e.g. sites 4, 5) are uniformly repulsive for P segregation. The most positive γ_{seg} (site 5, 0.277eV) is higher than that of Σ9 {221} GB, indicating a stronger P-GB interaction. More negative γ_{seg} and more core sites for preferential P segregation suggest that Σ27 {552} GB has a higher P gettering ability than Σ9 {221} GB. Apart from the core sites, four more sites (sites 21, 22, 21′, 22′) with negative γ_{seg}, adjacent to the core sites were also determined to be favorable for P segregation.

On the contrary, the segregation of As atoms at Σ27 {552} GB is much less energetically favorable than P atoms. As one can find in Fig. 2b, most of the core sites in Σ27 {552} GB possesses a positive γ_{seg}, while only 4 sites have negative γ_{seg} of negligible values. Such interaction behavior between As atoms and Si GBs without coordination defects is analogous with the predictions by Arias and Joannopoulos [65], wherein the segregation tendency of As towards Germanium Σ5 {310} tilt GB is less than 0.1 eV.

3.4 Σ3 {112} GBs

The (1×2) model of A-Σ3 {112} GB has 16 core sites (cf. Fig. 1d), within which 3 sites (sites 6, 7, 8) show negative γ_{seg} values, being attractive for P segregation. Site 7 exhibits the most negative γ_{seg}, -0.152 eV/atom. The less preferential segregation sites and less negative γ_{seg} suggest the P gettering ability of A-Σ3 {112} GB is much lower than Σ27 {552} GB. However, the segregation of As impurities

at A-Σ3 {112} GB is energetically unfavorable as suggested by the positive γ_{seg} at all core sites (cf. Fig. 2b). In contrast, much more pronounced P and As segregation can occur at the (1×2) model of S-Σ3 {112} GB. As one can find in Fig. 1c that S-Σ3 {112} GB has 6 potential core sites for segregation of P or As atoms. Among these sites, only one site (site 1) is calculated to be repulsive for P segregation. Site 5 in S-Σ3 {112} GB, adjacent to site 6 which has a pentavalent bonding coordination, was predicted to have the most negative γ_{seg} for P segregation, i.e. -0.613 eV/atom. Different from the P segregation, all the core sites in S-Σ3 {112} GB are attractive for As segregation as indicated by the calculated negative γ_{seg} (cf. Fig. 2b). Again, site 5 has the most negative γ_{seg}, i.e. -0.584 eV/atom, exhibiting the strongest sink strength for As impurities.

Fig. 3 presents the segregation profile of P and As along the (1×1) models of S- and A-Σ3 {112} GBs. As can be seen, two core sites (sites 1, 5) in S-Σ3 {112} GBs show prominent attraction for P and As segregation, with γ_{seg} value close to -0.6 eV/atom. In contrast, more than half of the 16 core sites in A-Σ3 {112} GBs show negative segregation energy for P and As. It is interesting to see that the γ_{seg} profiles of P and As along the (1×1) models of S- and A-Σ3 {112} GBs are similar to each other, in terms of preferential segregation sites and values of γ_{seg}. Furthermore, the (1×1) model of A-Σ3 {112} GB possesses more energetically favorable sites with more negative γ_{seg} values than the (1×2) model of A-Σ3 {112} GB for P and As segregation. This pronounced difference suggests that GB reconstruction may have prominent effect upon the segregation behaviors of P and As atoms.

3.5 Comparison with experimental results

3.5.1 Segregation of P, As at coherent Σ3 {111} GB

Ohno et al. [64] investigated the elemental distribution of impurity P at coherent Σ3 {111} twin boundary via APT and TEM, in which no segregation of P was detected. Using STEM analysis, Grovenor et al. [27] probed the As segregation at Si GBs and did not detect any As segregation at the Σ3 {111} GB. The predicted unfavorable P, As segregation at coherent Σ3 {111} GB in present work is in good agreement with the above experimental results. This should be attributed to the extremely

low γ_{GB} of Σ3 {111} GB, which is against any structural changes introduced by impurity segregation, as discussed in a previous work [35]. The unfavorable P, As segregation at Σ3 {111} GB indicates its intrinsically weak gettering ability of impurity atoms.

3.5.2 Segregation of P, As at other Σ GBs in Si

As demonstrated in the calculations, both P and As have a large driving force to segregate towards some specific Si GBs, e.g. S-Σ3 {112} GBs. Unfortunately, experimental results on P, As segregation at specific Σ GBs (except for Σ3 {111}) in Si has been few, which makes a direct comparison between the present calculation work and experimental results difficult. However, a large number of experimental studies by different approaches including APT [11, 12, 25, 26, 28], SIMS [26], AES [31, 66], STEM [27, 32] have shown significant segregation of P and As at Si GBs. Although the crystal structure and the type of the GBs in these experiments were not identified, most of them are supposed to be random or Σ GBs with more complex crystal structures than those simulated in the present work. Due to the size limit of supercells for DFT calculation, it is difficult to construct and investigate these complex GBs. However, these GBs can be considered as complex versions of Σ3 {112} GBs, containing more lattice distortions and defects with negative segregation energy. So the detected strong segregation of P and As in these GBs is in agreement with the present calculation results.

3.5.3 *Effect of dangling/extra bonds on GB segregation*

Experimental study on the effects of dangling/extra bonds in GBs on impurity segregation is not yet available. However, experimental results based on APT measurement have shown the strong segregation of P and As dopants at the interface between gate poly-Si film and gate oxide film in *n*-type MOSFET [11, 28, 67]. One can find the maximum concentration of the As dopants at the Si/SiO_2 interface is about 2 times as that along GBs in poly-Si gate while 20 times as that in the bulk of grain [28]. This can be well explained by the As segregation induced by dangling/extra bond effect predicted in this work. There is supposed to be a much higher density of dangling/extra bonds at the Si/SiO_2 interface than in Si GBs. More interestingly, the measured maximum concentration of P dopant at the Si/SiO_2 interface is just slightly higher than that along Si GBs [28]. Such behavior may also be

accounted for by the present calculation results, where the intrinsic lattice distortion at Si GBs is an important attraction source for P segregation but not for As. It is considered that the lattice distortion at the Si/SiO_2 interface and Si GBs has a more significant contribution to P segregation than dangling/extra bonds, which produces the comparable P enrichment level at Si/SiO_2 interface and Si GBs.

4. Discussion

The present calculations show apparently that only a fraction of the atomic sites along the Σ GBs are attractive for P segregation while the rest are not. Such a behavior is similar to the heterogeneous Fe segregation at CSL GBs in Si, predicted by Ziebarth et al. [58]. It is also interesting that the Σ3 {112} GBs have a significantly higher gettering ability for P, As than the other CSL GBs. The strong gettering ability of Σ3 {112} GBs was also recognized for other elements including C [63] and Fe [68]. The distinct segregation behavior of impurity atoms can be related to the high structural irregularity of Σ3 {112} GBs. Efforts have been made to find the correlation between γ_{seg} and structural characters of GB core sites, in terms of average bond length and angle, coordination number, etc. It is interesting to see that core sites with dangling bonds alongside the GBs ((1×1) models of S- and A-Σ3 {112} GBs) are always remarkably attractive for the segregation of P and As, and usually possess a γ_{seg} value of around -0.6 eV/atom. This interaction can be interpreted in terms of the intrinsic nature of P and As atoms. As group-V elements, P and As have a strong tendency to be three- or five-coordinated than to occupy a four-coordinated site in bulk Si, by which P or As become positive charged with their fifth free electron being contributed to the conduction band. However, Si atom, as a group-IV element, prefers to form saturated sp^3 tetrahedral bond rather than to be three-coordinated with a dangling bond. Thereby, P and As segregation from Si bulk lattice towards the core GB sites with dangling bonds can occur via the following reaction [69, 70]:

$$P(As)^{+}_{bulk} + Si^{-}_{GB} \rightarrow P(As)^{0}_{GB} + Si^{0}_{bulk} \quad (5)$$

This reaction, in which positively charged P or As substitutes the negative charged under-coordinated Si sites and produces electrically neutral P, As, and Si atoms, is energetically exothermic, since the

energy of ions on the left side of Eq. (5) is always higher than that on the right side. Eq. (5) can explain why GB defects containing under-coordinated Si atoms, with dangling bonds, can serve as efficient gettering/trapping sites for P and As impurities. It should be noted that Eq. (5) also involves the transformation of one P-Si bond to a new Si-Si bond, as well as charge redistribution, which is supposed to play a dominant role in yielding the driving force of P and As segregation to Si GBs.

Using the electron spin resonance (ESR) technique, the presence of dangling bond in Si GBs has been identified several decades before [33, 71], and the density of dangling bond in GBs of mc-Si films is estimated to be around 10^{-12} cm^{-2} [33, 72, 73]. As will be demonstrated in the following part, atomic sites with dangling bonds are strongly attractive for the segregation of P and As impurities. However, as discussed in Refs. [27, 74], most of the dangling bonds at the GBs which trap carriers are not detectable by ESR measurement. Trap centers, on the contrary, is the major cause for ESR signal. This could be an indication that the dangling bond density along the Si GBs could be more than the magnitude of 10^{-12} cm^{-2}. As a result of the strong attraction between P or As impurities and under-coordinated Si sites, these high density of dangling bonds are considered to contribute substantially to the prominent P and As segregations along Si GBs.

On the other hand, the core sites along Σ3 {111}, Σ9 {221}, and Σ27 {552} GBs are all four coordinated, while atomic sites with dangling bonds do not exist in these GBs. Still, calculations show that alien P impurity has considerable driving force to segregate to Σ9 {221} and Σ27 {552} GBs. However, no core sites on these GBs show strongly negative segregation energy values for As impurity. Such a manifest difference in segregation tendency between P and As should be associated with the difference in atomic radius of the two elements, which results in a distinct lessening of elastic lattice strain and atomic bonding energy of the GBs by the introduction of a misfitting dopant atom. Actually, these three types of GBs, i.e. Σ3 {111}, Σ9 {221} and Σ27 {552}, all have lattice distortion in reference to bulk Si, and the extent of which increases with Σ values, as shown in a previous work [35]. Here, Σ27 {552} GB bears the largest lattice distortion energy, contributed by the periodic localized compressed and tensile areas along the GB [35]. The higher intrinsic lattice distortion of the GB would

generate its inherent higher gettering ability of P atoms. This can well explain the higher P segregation tendency along Σ27 {552} GB than Σ9 {221} GB as predicted in the present work.

It is worth noting that the segregation behavior of P is similar to that of C along Σ9 {221} and Σ27 {552} GBs [35], wherein P and C atoms incline to reside at some particular sites (e.g. site 5 in Σ9 {221} GB, site 12 in Σ27 {552} GB) alongside the GBs. These sites refer to a compressed state in the GB core region. Therefore, the similarity in preferential segregation site between C and P can be ascribed to the atomic size effect. Fig. 4 shows the bonding length change of site 12 in Σ27 {552} GB due to P, C, and As segregation. One can find that the substitution of Si atom at this core site by an atom with a smaller atomic radius, C or P, can release the elastic strain energy localized in the five-fold ring. In other words, the compressive lattice distortion provides the driving force for C and P segregation. However, C has an even smaller atomic radius than P, its segregation would release more elastic strain, and thus more negative γ_{seg} (-0.524 vs. -0.4 eV/atom, cf. Fig. 4). Thereby a direct correlation exists between the atomic size and γ_{seg}, i.e. the smaller the atomic size of impurity dopants, the more negative of γ_{seg}, and vice versa. On the other hand, As has a slightly larger atomic size than Si. A substitution of the core Si atom by As will slightly increase the average bonding length, thus lattice distortion can hardly yield the driving force for its segregation along these GBs. Even for Σ27 {552} GB, which has a larger intrinsic lattice distortion, is still not energetically favorable for the segregation of As atoms (cf. Fig. 4). The segregation behavior of P and As dopants along the (1×1) models of A-Σ3 {112} GB further evidences the contribution of GB lattice distortion to the driving force for P segregation. As can be seen in Fig. 3a, sites 5-8 in A-Σ3 {112} GB bear negative γ_{seg} for P segregation, among which, site 7 has the most negative value, i.e. -0.366 eV/atom. However, the γ_{seg} values for As segregation at these sites are much less pronounced (cf. Fig. 3b), indicating that the intrinsic lattice distortion has much less effect on the As segregation at the GB.

Fig. 5 displays the total density of states (TDOS) of bulk Si, Σ3 {111}, Σ9 {221} and Σ27 {552} GBs. As can be seen, evident bandgap exists in the TDOS of bulk Si, Σ3 {111}, Σ9 {221}, Σ27 {552} GBs, and there are no energy states in the bandgap, being in accordance with the absence of dangling

bonds in these GBs. Fig. 6a shows the TDOS of S- and A-Σ3 {112} GBs with reconstruction along the <1$\bar{1}$0> direction, in which one can find that deep states exist in the bandgap in S-Σ3 {112} GB. Further calculations of the partial density of states (PDOS) at different core sites at the GB reveal that only Si atoms at site 5 generate these strong deep states (cf. Fig. 6b), contributing to the most part of the deep levels in the bandgap in S-Σ3 {112} GB. Fig. 6c-d shows the partial charge density with the energy states in between the valence band maximum (VBM) and conduction band minimum (CBM), which is localized mainly at atomic site 5 at the GB. Such behavior is consistent with the PDOS result in Fig. 6b, indicating that the deep levels in the bandgap in S-Σ3 {112} GB are mainly associated with atomic site 5. It is worth noting that the generation of these levels around site 5 is attributed to the extra bonds of core site 6 at the GB. These results bear nice agreement with the calculations by Feng et al. [75] and Sakaguchi et al. [76], wherein new states were predicted in the bandgap of TDOS. Another interesting phenomenon is that site 5 in S-Σ3 {112} GB is strikingly attractive for the segregation of P and As atoms, even though it is four-coordinated and not much distorted. Such high segregation inclination must be linked to the inherent deep levels at site 5, originated from the extra bonds of adjacent site 6, which can localize electrons and make site 5 serve as efficient P and As traps at the GB.

Deep levels in the bandgap which result in significant P and As segregation, can be created not only by the extra bonds, but also by dangling bonds of the atomic sites at the Si GBs. Fig. 7a shows the TDOS of CSL (1×1) model of S- and A-Σ3 {112} GBs without reconstruction along the <1$\bar{1}$0> direction. Apparently, both GBs have deep levels in the bandgap of TDOS. It is worth noting that the deep levels in S-Σ3 {112} GBs have a mixed nature, which are produced both by the dangling bonds of sites 1, and by the extra bonds of sites 6 (cf. Fig. 7a). However, the deep levels in A-Σ3 {112} GBs are solely created by the Si dangling bonds of sites 2 and 9, as evidenced by the deep states between VBM and CBM in the PDOS of sites 2 and 9 in A-Σ3 {112} GBs (cf. Fig. 7b). Partial charge density with energy states in between VBM and CBM as indicated in Fig. 7c-d also demonstrates the localized electrons at the three coordinated sites 2 and 9, which contribute to the major part of deep levels in the bandgap of A-Σ3 {112} GBs. Calculations show that sites 2 and 9 in the (1×1) model of A-Σ3 {112} GB exhibit

extremely high attractive strength for P and As segregation, which must be attributed to their intrinsic deep levels in the bandgap. These deep levels created either by extra bonds or dangling bonds can trap or localize electrons and make these GB sites exhibit a high attractive binding energy for *n*-type dopants. As a result of the deep levels, substantial P and As segregations at the S- and A-Σ3 {112} GBs can be expected.

The above results indicate that the driving force for the substantial P and As segregation along Si GBs is strongly linked with the intrinsic character of the GBs. As illustrated in the schematic in Fig. 8, the lattice distortion and the deep levels in the bandgap of density of states produced by extra or dangling bonds of the core sites dominate the GB segregation of impurity elements. For impurity elements with atomic size much different from Si, for instance P and C, the GB core sites with large lattice distortion are energetically favorable gettering sites. However, for atoms such as As, with a similar size to Si, the lattice distortion of core sites at GBs has a negligible influence on the segregation energy. Substantial P and As segregations along Si GBs should also be ascribed to the deep levels in the bandgap of density of states produced by extra or dangling bonds of the GB core sites. It is worth noting that the Σ3 {111} GB, with the least lattice distortion and no deep levels in bandgap, has no significant interaction with P and As atoms. Thereby, a high fraction of this GB would effectively suppress the heterogeneous distribution of P and As impurities in *n*-type mc-Si. This means that a high fraction of Σ3 {111} GB is favorable for *n*-type mc-Si materials to achieve a better electrical performance. Another alternative to reduce the P and As agglomeration at Si GBs is to eliminate the deep states in the bandgap of density of states, which can be enforced with hydrogen passivation. As reported, hydrogenation is an efficient routine to reduce the density of dangling bonds in mc-Si based materials by orders of magnitude [73, 77-80], which is a major cause of the deep levels in the bandgap. With increasing passivation time, hydrogenation can decrease the dangling bond density in mc-Si till a residual defect concentration level [73, 80]. Nevertheless, deep levels ascribed to the extra bonds in the GB cannot be simply passivated with hydrogenation. However, as demonstrated by Feng et al. [75], the complete passivation of such deep levels can be achieved via a vacancy aided hydrogenation.

Apart from the Σ GBs as investigated in the present work, random GBs, high Σ value GBs, as well as low angle GBs also exist in mc-Si, and can account for a large GB population [81, 82]. A deeper understanding on the P, As segregation at Si GBs will require an extension of the present calculations of segregation behaviors from low-Σ GBs to high Σ value GBs, low angle GBs and even random GBs in mc-Si. However, the complex of atomic structures of such GBs need large supercells which make the investigation of segregation via first-principles calculations quite challenging. Yet the knowledge of P, As segregation behavior at low-Σ Si GBs in the present work is considered to yield a fundamental understanding towards their segregations along other GBs in mc-Si. The random GBs can be considered as composed of higher density of Si defects, which are characterized by large density of distorted bonds and over-/under- coordinated Si atoms. As demonstrated in the present work, such defects can induce lattice distortion and deep levels in the bandgap of density of states which can drive P and As segregation at the GBs. This can account for the frequently observed substantial P and As segregation at random GBs in mc-Si as reported in various experiments [11, 12, 25, 26, 28]. It is documented in a variety of experiments that the high-Σ GBs turn to possess a higher level of bond distortion compared with low-Σ GBs, resulting in higher gettering ability of impurity elements [83, 84]. The P and As segregations at these high-Σ GBs in mc-Si are proposed to be similar to the segregation behavior at low-Σ GBs as investigated in the present work, while higher level of P segregation at high-Σ GBs can be expected due to the higher density of lattice distortion sites in the GBs. However, the segregation of P and As at low angle GBs in mc-Si are supposed to be different since such GBs are composed of periodic dislocation arrangement. The segregation behavior at low angle GBs can be anticipated on basis of the P, As segregation at the dislocations [85, 86]. In addition, elastic strain field induced by lattice distortion around the dislocations can play an important role in the P segregation.

5. Conclusion

To sum up, systematic first-principles calculations on the segregation behaviors of substitutional dopants P and As at a set of CSL Si GBs, including Σ3 {111}, Σ9 {221}, Σ27 {552}, Σ3 {112}, have been conducted for the sake of better understanding of the fundamental mechanisms inducing P, As segregation at Si GBs. Preferential segregation of P and As atoms at specific atomic

sites of these Si GBs is predicted, which is consistent with the apparent P, As enrichment at Si GBs observed in experiments. On basis of the calculations in the present work, the following conclusions have been addressed.

- The Σ3 {111} GB is not able to getter P, As atoms, due to its intrinsic low energy GB structure. Preferential P segregation can occur at the GBs of Σ3 {112}, Σ9 {221} and Σ27 {552}. However, As segregation at Σ9 {221} and Σ27 {552} GBs is energetically unfavorable.
- Three variants of Σ3 {112} GBs containing deep levels in the bandgap of density of states, which are produced by extra or dangling bonds in the GBs, show prominent attraction for both P and As segregation.
- The segregation behavior of P atoms along Si GBs suggests that the driving force for P segregation is ascribed to the intrinsic characters of GBs, i.e. the lattice distortion and deep levels in the bandgap of density of states.
- In contrast, As segregation is mainly caused by the GB deep levels, whereas GB lattice distortion hardly takes effect, as a result of the similar atomic size between As and Si.

In general, this work demonstrates that the substitutional impurity segregation at Si GBs is strongly linked to the GB characteristics, as well as the properties of impurity atoms. The intrinsic GB lattice distortion plays an important role in driving segregation of impurity elements which have much different atomic size from Si, e.g. P and C atoms. This GB characteristic has much less effect on segregation when it comes to the impurity element possessing similar atomic size with Si. For group-V impurity elements, the deep levels in the bandgap of density of states, produced either by dangling or extra bonds, serves as another important driving force for the substantial P, As segregation along Si GBs. The present predictions are supposed to be helpful for the improvement of processing techniques in suppressing P and As segregation in Si wafers to achieve more uniform dopant distribution for the sake of enhanced electrical properties of nano-devices.

Acknowledgement

This work is financially supported under the FRINATEK project 'BENTMAT' (project number 222173) from the Research Council of Norway. Computation time from the NOTUR consortium (project number: nn9347k) is gratefully acknowledged.

References

[1] P.V. Liddicoat, X.-Z. Liao, Y.H. Zhao, Y.T. Zhu, M.Y. Murashkin, E.J. Lavernia, R.Z. Valiev, S.P. Ringer, Nanostructural hierarchy increases the strength of aluminium alloys, Nat. Commun., 1:63 (2010) 1-7.

[2] D. Raabe, M. Herbig, S. Sandlöbes, Y. Li, D. Tytko, M. Kuzmina, D. Ponge, P.-P. Choi, Grain boundary segregation engineering in metallic alloys: A pathway to the design of interfaces, Curr. Opin. Solid. State. Mater Sci., 18 (2014) 253–261.

[3] M.A. Gibson, C.A. Schuh, Segregation-induced changes in grain boundary cohesion and embrittlement in binary alloys, Acta. Mater., 95 (2015) 145-155.

[4] P. Lejček, M. Šob, V. Paidar, Interfacial segregation and grain boundary embrittlement: An overview and critical assessment of experimental data and calculated results, Prog. Mater. Sci., 87 (2017) 83–139.

[5] A. Khalajhedayati, Z.L. Pan, T.J. Rupert, Manipulating the interfacial structure of nanomaterials to achieve a unique combination of strength and ductility, Nat. Commun., 7 (2016) 10802.

[6] D.D. Zhao, O.M. Løvvik, K. Marthinsen, Y.J. Li, Segregation of Mg, Cu and their effects on the strength of Al Σ5 (210)[001] symmetrical tilt grain boundary, Acta. Mater., 145 (2018) 235-246.

[7] R. Kirchheim, Reducing grain boundary, dislocation line and vacancy formation energies by solute segregation. I. Theoretical background, Acta Mater., 55 (2007) 5129–5138.

[8] R. Raghunathan, E. Johlin, J.C. Grossman, Grain Boundary Engineering for Improved Thin Silicon Photovoltaics, Nano Lett., 14 (2014) 4943−4950.

[9] A. Stoffers, O. Cojocaru-Mirédin, W. Seifert, S. Zaefferer, S. Riepe, D. Raabe, Grain boundary segregation in multicrystalline silicon: correlative characterization by EBSD, EBIC, and atom probe tomography, Prog. Photovolt: Res. Appl., 23 (2015) 1742–1753.

[10] Y. Ohno, K. Inoue, K. Fujiwara, M. Deura, K. Kutsukake, I. Yonenaga, Y. Shimizu, K. Inoue, N. Ebisawa, Y. Nagai, Three-dimensional evaluation of gettering ability for oxygen atoms at small-angle tilt boundaries in Czochralski-grown silicon crystals, Appl. Phys. Lett., 106 (2015) 251603.

[11] K. Inoue, F. Yano, A. Nishida, H. Takamizawa, T. Tsunomura, Y. Nagai, M. Hasegawa, Dopant distribution in gate electrode of n - and p -type metal-oxide-semiconductor field effect transistor by laser-assisted atom probe, Appl. Phys. Lett., 95 (2009) 043502.

[12] D. Blavette, S. Duguay, Investigation of dopant clustering and segregation to defects in semiconductors using atom probe tomography, J. Appl. Phys., 119 (2016) 181502.

[13] O. Hazut, A. Agarwala, I. Amit, T. Subramani, S. Zaidiner, Y. Rosenwaks, R. Yerushalmi, Contact Doping of Silicon Wafers and Nanostructures with Phosphine Oxide Monolayers, ACS Nano, 6 (2012) 10311–10318.

[14] Z.Y. Sun, O. Hazut, B.-C. Huang, Y.-P. Chiu, C.-S. Chang, R. Yerushalmi, L.J. Lauhon, D.N. Seidman, Dopant Diffusion and Activation in Silicon Nanowires Fabricated by ex Situ Doping: A Correlative Study via Atom-Probe Tomography and Scanning Tunneling Spectroscopy, Nano Lett, 16 (2016) 4490−4500.

[15] I. Amit, N. Jeon, L.J. Lauhon, Y. Rosenwaks, Impact of Dopant Compensation on Graded p−n Junctions in Si Nanowires, ACS Appl. Mater. Interfaces, 8 (2016) 128−134.

[16] E. Koren, J.K. Hyun, U. Givan, E.R. Hemesath, L.J. Lauhon, Y. Rosenwaks, Obtaining Uniform Dopant Distributions in VLS-Grown Si Nanowires, Nano Lett., 11 (2011) 183–187.

[17] E. Koren, N. Berkovitch, Y. Rosenwaks, Measurement of Active Dopant Distribution and Diffusion in Individual Silicon Nanowires, Nano Lett., 10 (2010) 1163–1167.

[18] O. Hazut, B.-C. Huang, A. Pantzer, I. Amit, Y. Rosenwaks, A. Kohn, C.-S. Chang, Y.-P. Chiu, R. Yerushalmi, Parallel p-n Junctions across Nanowires by One-Step Ex Situ Doping, ACS Nano, 8 (2014) 8357–8362.

[19] B. Han, H. Takamizawa, Y. Shimizu, K. Inoue, Y. Nagai, F. Yano, Y. Kunimune, M. Inoue, A. Nishida, Phosphorus and boron diffusion paths in polycrystalline silicon gate of a trench-type three-dimensional metal-oxide-semiconductor field effect transistor investigated by atom probe tomography, Appl. Phys. Lett., 107 (2015) 023506.

[20] K. Thompson, P.L. Flaitz, P. Ronsheim, D.J. Larson, T.F. Kelly, Imaging of Arsenic Cottrell Atmospheres Around Silicon Defects by Three-Dimensional Atom Probe Tomography, Science, 317 (2007) 1370-1374.

[21] K. Thompson, J.H. Booske, D.J. Larson, T.F. Kelly, Three-dimensional atom mapping of dopants in Si nanostructures, Appl. Phys. Lett., 87 (2005) 052108.

[22] P.A. Stolk, F.P. Widdershoven, D.B.M. Klaassen, Modeling Statistical Dopant Fluctuations in MOS Transistors, IEEE Trans. Electron Devices, 45 (1998) 1960-1971.

[23] T. Buonassisi, A.A. Istratov, M.A. Marcus, B. Lai, Z.H. Cai, S.M. Heald, E.R. Weber, Engineeringmetal-impurity nanodefects for low-cost solar cells, Nature Mater., 4 (2005) 676-679.

[24] M.R. Castell, D.A. Muller, P.M. Voyles, Dopant mapping for the nanotechnology age, Nature Mater., 2 (2003) 129-131.

[25] K. Inoue, F. Yano, A. Nishida, H.Takamizawa, T. Tsunomura, Y. Nagai, M. Hasegawa, Dopant distributions in n-MOSFETstructure observed by atom probe tomography, Ultramicroscopy, 109 (2009) 1479–1484.

[26] S. Duguay, A. Colin, D. Mathiot, P. Morin, D. Blavette, Atomic-scale redistribution of dopants in polycrystalline silicon layers, J . Appl. Phys., 108 (2010) 034911.

[27] C.R.M. Grovenor, P.E. Batson, D.A. Smith, C. Wong, As segregation to grain boundaries in Si, Phil. Mag., 50 (1984) 409-423.
[28] K. Inoue, F. Yano, A. Nishida, T. Tsunomura, T. Toyama, Y. Nagai, M. Hasegawa, Three dimensional characterization of dopant distribution in polycrystalline silicon by laser-assisted atom probe, Appl. Phys. Lett., 93 (2008) 133507.
[29] A. Asenov, S. Saini, Suppression of Random Dopant-Induced Threshold Voltage Fluctuations in Sub-0.1-m MOSFET's with Epitaxial and -Doped Channels, IEEE Trans. Electron Devices, 46 (1999) 1718-1724.
[30] S. Duguay, T. Philippe, F. Cristiano, D. Blavette, Direct imaging of boron segregation to extended defects in silicon, Appl. Phys. Lett., 97 (2010) 242104.
[31] L.L. Kazmerski, P.J. Ireland, T.F. Ciszek, Evidence for the segregation of impurities to grain boundaries in multigrained silicon using Auger electron spectroscopy and secondary ion mass spectroscopy, Appl. Phys. Lett., 36 (1980) 323-325.
[32] J.H. Rose, R. Gronsky, Scanning transmission electron microscope microanalytical study of phosphorus segregation at grain boundaries in thin-film silicon, Appl. Phys. Lett., 41 (1982) 993-995.
[33] C.R.M. Grovenor, Grain boundaries in semiconductors, J. Phys. C: Solid State Phys., 18 (1985) 4079-4119.
[34] S. Nédélec, D. Mathiot, Kinetics of arsenic segregation at grain boundaries in polycrystalline silicon, Semicond. Sci. Technol., 12 (1997) 1438–1445.
[35] D.D. Zhao, Y.J. Li, Lattice distortion induced site dependent carbon gettering at twin boundaries in silicon, J. Alloys. Comp., 712 (2017) 599-604.
[36] V.I. Razumovskiy, S.V. Divinski, L. Romaner, Solute segregation in Cu: DFT vs. Experiment, Acta. Mater., 147 (2018) 122-132.
[37] M.M. Mandurah, K.C. Saraswat, C.R. Helms, T.I. Kamins, Dopant segregation in polycrystalline silicon, J . Appl. Phys., 51 (1980) 5755-5763.
[38] X.B. Wu, Y.-W. You, X.-S. Kong, J.-L. Chen, G.-N. Luo, G.-H. Lu, C.S. Liu, Z.G. Wang, First-principles determination of grain boundary strengthening in tungsten: Dependence on grain boundary structure and metallic radius of solute, Acta. Mater., 120 (2016) 315-326.
[39] T. Tsuru, H. Somekawa, D.C. Chrzan, Interfacial segregation and fracture in Mg-based binary alloys: Experimental and first-principles perspective, Acta. Mater., 151 (2018) 78-86.
[40] M.F. Chisholm, A. Maiti, S.J. Pennycook, S.T. Pantelides, Atomic Configurations and Energetics of Arsenic Impurities in a Silicon Grain Boundary, Phys. Rev. Lett., 81 (1998) 132-135.
[41] A. Maiti, M.F. Chisholm, S.J. Pennycook, S.T. Pantelides, Dopant Segregation at Semiconductor Grain Boundaries through Cooperative Chemical Rebonding, Phys. Rev. Lett., 77 (1996) 1306-1309.
[42] M.G. Tsoutsouva, T. Riberi-Béridot, G. Regula, G. Reinhart, J. Baruchel, F. Guittonneau, L. Barrallier, N. Mangelinck-Noël, In situ investigation of the structural defect generation and evolution during the directional solidification of <110> seeded growth Si, Acta Mater., 115 (2016) 210-223.

[43] V.A. Oliveira, B. Marie, C. Cayron, M. Marinova, M.G. Tsoutsouva, H.C. Sio, T.A. Lafford, J. Baruchel, G. Audoit, A. Grenier, T.N. Tran Thi, D. Camel, Formation mechanism and properties of twinned structures in (111) seeded directionally solidified solar grade silicon, Acta Mater., 121 (2016) 24-36.
[44] H.K. Lin, C.W. Lan, Revisiting the twinning mechanism in directional solidification of multi-crystalline silicon sheet, Acta Mater., 131 (2017) 1-10.
[45] T. Jain, H.K. Lin, C.W. Lan, Twinning mechanism at three-grain tri-junction during directional solidification of multi-crystalline silicon, Acta Mater., 144 (2018) 41-50.
[46] P.E. Blöchl, Projector augmented-wave method, Phys. Rev. B, 50 (1994) 17953-17979.
[47] G. Kresse, D. Joubert, From ultrasoft pseudopotentials to the projector augmented-wave method, Phys. Rev. B, 59 (1999) 1758-1775.
[48] J.P. Perdew, K. Burke, M. Ernzerhof, Generalized Gradient Approximation Made Simple, Phys. Rev. Lett., 77 (1996) 3865.
[49] G. Kresse, J. Furthmüller, Efficiency of ab-initio total energy calculations for metals and semiconductors using a plane-wave basis set, Comp. Mater. Sci., 6 (1996) 15-50.
[50] G. Kresse, J. Furthmüller, Efficient iterative schemes for ab initio total-energy calculations using a plane-wave basis set, Phys. Rev. B, 54 (1996) 11169-11186.
[51] H.J. Monkhorst, J.D. Pack, Special points for Brillouin-zone integrations, Phys. Rev. B, 13 (1976) 5188-5192.
[52] P.E. Blöchl, O. Jepsen, O.K. Andersen, Improved tetrahedron method for Brillouin-zone integrations, Phys. Rev. B, 49 (1994) 16223-16233
[53] B. Cunningham, H.P. Strunk, D.G. Ast, High resolution electron microscopy of a Σ=27 boundary in Silicon, Scr. Metall., 16 (1982) 349-352.
[54] M.D. Vaudin, B. Cunningham, D.G. Ast, The structure of second and third order twin boundaries in Silicon, Scr. Metall., 17 (1983) 191-198.
[55] H.J. Queisser, Properties of Twin Boundaries in Silicon, J. Electrochem. Soc., 110 (1963) 52-56.
[56] M. Kohyama, R. Yamamoto, M. Doyama, Structures and Energies of Symmetrical <011> Tilt Grain Boundaries in Silicon, Phys. Stat. Sol. (b), 137 (1986) 11-20.
[57] P. Käshammer, T. Sinno, Interactions of twin boundaries with intrinsic point defects and carbon in silicon, J. Appl. Phys., 114 (2013) 083505.
[58] B. Ziebarth, M. Mrovec, C. Elsässer, P. Gumbsch, Interstitial iron impurities at grain boundaries in silicon: A first-principles study, Phys. Rev. B, 91 (2015) 035309.
[59] R. Yu, H. Wu, J.D. Wang, J. Zhu, Strain Concentration at the Boundaries in 5-Fold Twins of Diamond and Silicon, ACS Appl. Mater. Interfaces, 9 (2017) 4253-4258.
[60] H. Sawada, H. Ichinose, M. Kohyama, Gap states due to stretched bonds at the (112) Σ3 boundary in diamond, J. Phys.: Condens. Matter, 19 (2007) 026223.

[61] L. Cartz, S.R. Srinivasa, R.J. Riedner, J.D. Jorgensen, T.G. Worlton, Effect of pressure on bonding in black phosphorus, J. Chem. Phys., 71 (1979) 1718-1721.
[62] H. Krebs, W. Holz, K.H. Worms, Über die Struktur und die Eigenschaften der Halbmetalle, X. Eine Neue Rhombische Arsenmodifikation und Ihre Mischkristallbildung mit Schwarzem Phosphor, Chem. Ber., 90 (1957) 1031-1037.
[63] D.D. Zhao, Y.J. Li, Carbon segregation at Σ3 {112} grain boundaries in silicon, Comp. Mater. Sci., 143 (2018) 80–86.
[64] Y. Ohno, K. Inoue, Y. Tokumoto, K. Kutsukake, I. Yonenaga, N. Ebisawa, H. Takamizawa, Y. Shimizu, K. Inoue, Y. Nagai, H. Yoshida, S. Takeda, Three-dimensional evaluation of gettering ability of Σ3 {111} grain boundaries in silicon by atom probe tomography combined with transmission electron microscopy, Appl. Phys. Lett., 103 (2013) 102102.
[65] T.A. Arias, J.D. Joannopoulos, Ab Initio Prediction of Dopant Segregation at Elemental Semiconductor Grain Boundaries without Coordination Defects, Phys. Rev. Lett., 69 (1992) 3330-3333.
[66] C.Y. Wong, C.R.M. Grovenor, P.E. Batson, D.A. Smith, Effect of arsenic segregation on the electrical properties of grain boundaries in polycrystalline silicon, J. Appl. Phys., 57 (1985) 438-442.
[67] A.D. Giddings, S. Koelling, Y. Shimizu, R. Estivill, K. Inoue, W. Vandervorst, W.K. Yeoh, Industrial application of atom probe tomography to semiconductor devices, Scr. Mater., 148 (2018) 82–90.
[68] B. Chen, J. Chen, T. Sekiguchi, M. Saito, K. Kimoto, Structural characterization and iron detection at Σ3 grain boundaries in multicrystalline silicon, J. Appl. Phys., 105 (2009) 113502.
[69] J. Dabrowski, R.A. Casali, H.-J. Müssig, R. Baierle, M.J. Caldas, V. Zavodinsky, Mechanism of dopant segregation to SiO2/Si(001) interfaces, J. Vac. Sci. & Tech. B, 18 (2000) 2160-2164.
[70] J. Dabrowski, H.-J. Müssig, V. Zavodinsky, R. Baierle, M.J. Caldas, Mechanism of dopant segregation to SiO2/Si(001) interfaces, Phys. Rev. B, 65 (2002) 245305.
[71] P.M. Lenahan, W.K. Schubert, Spin dependent trapping at a silicon grain boundary, Solid. State. Comm., 47 (1983) 423-425.
[72] G. Harbeke, Polycrystalline Semiconductors, Electronic States at Grain Boundaries in Semiconductors, 57 (1984) 95-117.
[73] K. von Maydell, N.H. Nickel, Hydrogen equilibration in polycrystalline silicon, Appl. Phys. Lett., 90 (2007) 132117.
[74] P.M. Lenahan, W.K. Schubert, Effects of light and modulation frequency on spin-dependent trapping at silicon grain boundaries, Phys. Rev. B, 30 (1984) 1544-1546.
[75] C.B. Feng, J.L. Nie, X.T. Zu, M.M. Al-Jassim, Y.F. Yan, Structure and effects of vacancies in Σ3 (112) grain boundaries in Si, J. Appl. Phys., 106 (2009) 113506.
[76] N. Sakaguchi, H. Ichinose, S. Watanabe, Atomic Structure of Faceted Σ3 CSL Grain Boundary in Silicon: HRTEM and Ab-initio Calculation, Mater. Trans., 48 (2007) 2585-2589.

[77] N.M. Johnson, D.K. Biegelsen, M.D. Moyer, Deuterium passivation of grain-boundary dangling bonds in silicon thin films, Appl. Phys. Lett., 40 (1982) 882-884.
[78] N.H. Nickel, N.M. Johnson, W.B. Jackson, Hydrogen passivation of grain boundary defects in polycrystalline silicon thin films, Appl. Phys. Lett., 62 (1993) 3285-3287.
[79] B. Sopori, Silicon Solar-Cell Processing for Minimizing the Influence of Impurities and Defects, J. Electron. Mater., 31 (2002) 972-980.
[80] L.P. Scheller, M. Weizman, P. Simon, M. Fehr, N.H. Nickel, Hydrogen passivation of polycrystalline silicon thin films, J . Appl. Phys., 112 (2012) 063711.
[81] R.R. Prakash, K. Jiptner, J. Chen, Y. Miyamura, H. Harada, T. Sekiguchi, Grain boundary interactions in multicrystalline silicon grown from small randomly oriented seeds, Appl. Phys. Express, 8 (2015) 035502.
[82] Y.M. Yang, A. Yu, B. Hsu, W.C. Hsu, A. Yang, C.W. Lan, Development of high-performance multicrystalline silicon for photovoltaic industry, Prog. Photovolt: Res. Appl., 23 (2015) 340–351.
[83] J. Chen, T. Sekiguchi, D. Yang, F. Yin, K. Kido, S. Tsurekawa, Electron-beam-induced current study of grain boundaries in multicrystalline silicon, J. Appl. Phys., 96 (2004) 5490-5495.
[84] T. Buonassisi, A.A. Istratov, M.D. Pickett, M.A. Marcus, T.F. Ciszek, E.R. Weber, Metal precipitation at grain boundaries in silicon: Dependence on grain boundary character and dislocation decoration, Appl. Phys. Lett., 89 (2006) 042102.
[85] K. Sumino, I. Yonenaga, Interactions of Impurities with Dislocations: Mechanical Effects, Solid State Phenomena, 85-86 (2002) 145-176.
[86] I. Yonenaga, Dislocation–impurity interaction in Si, Mater. Sci. Eng. B, 124-125 (2005) 293–296.

Table 1. Grain boundary energy γ_{GB} (unit: mJ/m^2) of Σ3 {111}, Σ9 {221}, Σ27 {552} and Σ3 {112} GBs.

Grain boundaries	Misorientation angle, θ	Number of atoms	γ_{GB}, mJ/m^2
Σ3 {111} GB	**70.53°**	**96**	**[a]0.014**
S-Σ3 {112} GB (1×2) model	**109.47°**	**96**	**[b]0.658**
A-Σ3 {112} GB (1×2) model	**109.47°**	**136**	**[b]0.363**
S-Σ3 {112} GB (1×1) model	**109.47°**	**96**	**0.916**
A-Σ3 {112} GB (1×1) model	**109.47°**	**92**	**0.908**
Σ9 {221} GB	**38.94°**	**136**	**[a]0.183**
Σ27 {552} GB	**31.59°**	**216**	**[a]0.359**

[a]Values taken from Ref. [35].

[b]Values taken from Ref. [63].

Figures

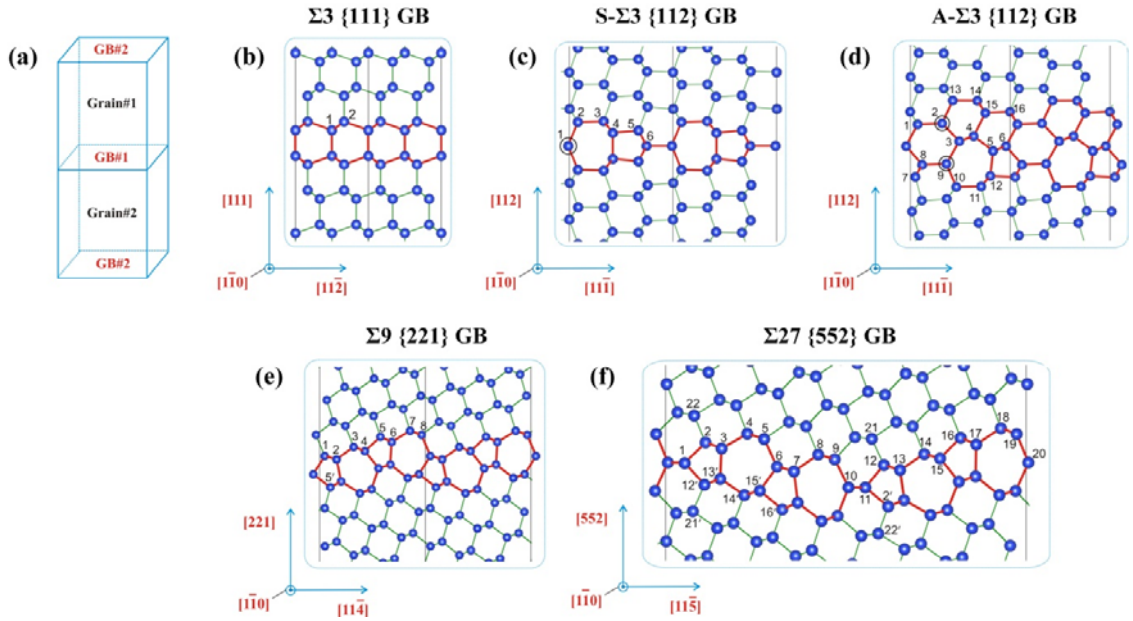

Fig. 1. (a) Bi-crystal supercell containing two GBs and two micro-grains, utilized in the simulations. Structures of (b) Σ3 {111}, (c) S- and (d) A-Σ3 {112}, (e) Σ9 {221} and (f) Σ27 {552} CSL GBs in Si as projected in the <1$\bar{1}$0> direction. The core sites of GBs for potential phosphorus and arsenic segregation are marked out with numbers. Black circles indicate the atomic sites in S- and A-Σ3 {112} GBs which have dangling bond in their respective (1×1) GB models.

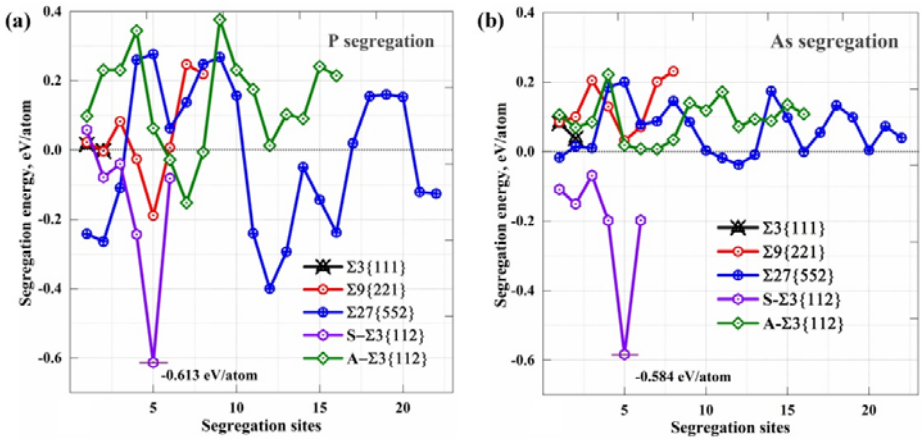

Fig. 2. Segregation energy of P and As atoms at the core sites of (a) Σ3 {111}, Σ9 {221}, Σ27 {552}, S- and A-Σ3 {112} GBs in Si. The S- and A-Σ3 {112} GBs are the CSL (1×2) models, which have bond reconstruction along the <1$\bar{1}$0> direction. The energy unit is in eV/atom. The segregation sites for each GB are as indicated in Figure 1.

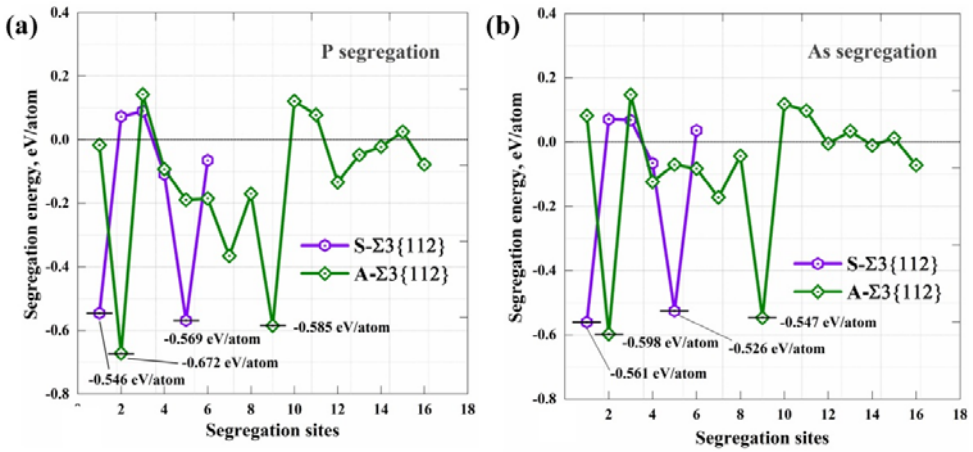

Fig. 3. Segregation energy of P and As atoms at the core sites of (1×1) models of S- and A-Σ3 {112} GBs in Si, which are without structural reconstruction along the <1$\bar{1}$0> direction. The energy unit is in eV/atom. The segregation sites for each GB are as indicated in Figure 1.

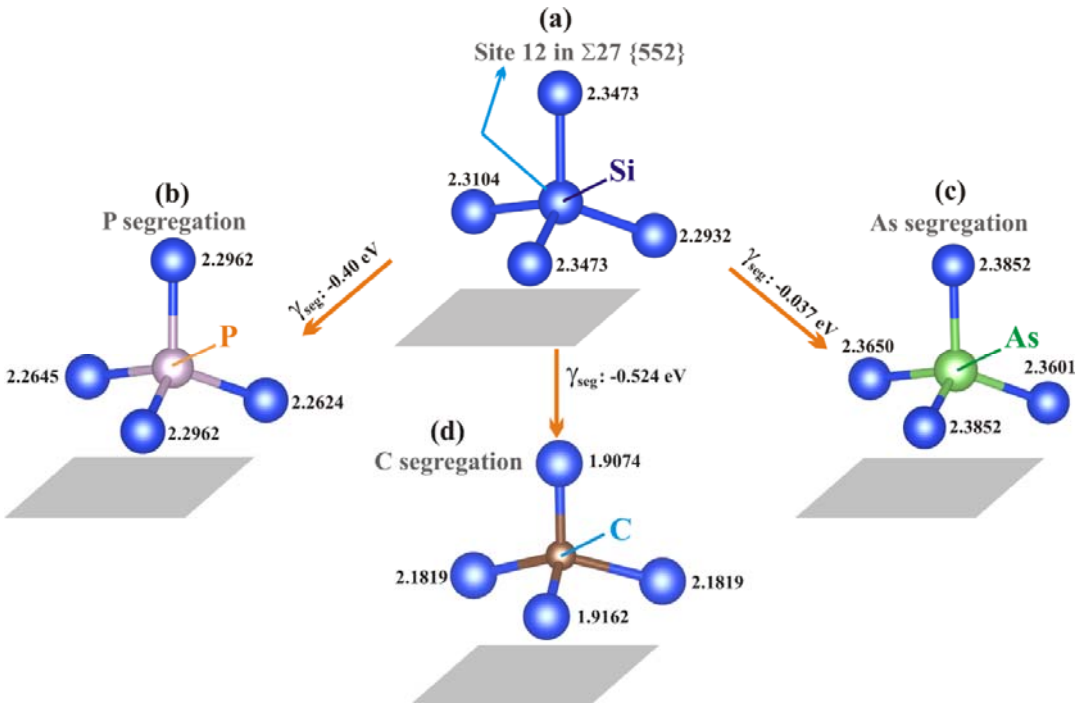

Fig. 4. (a) Bond length (unit: Å) of site 12 in pristine Σ27 {552} GB, (b) bond length of site 12 in Σ27 {552} GB with P segregation, (c) with As segregation, (d) with C segregation. The corresponding segregation energy γ_{seg} are also as indicated. Dataset of C segregation is from Ref. [35].

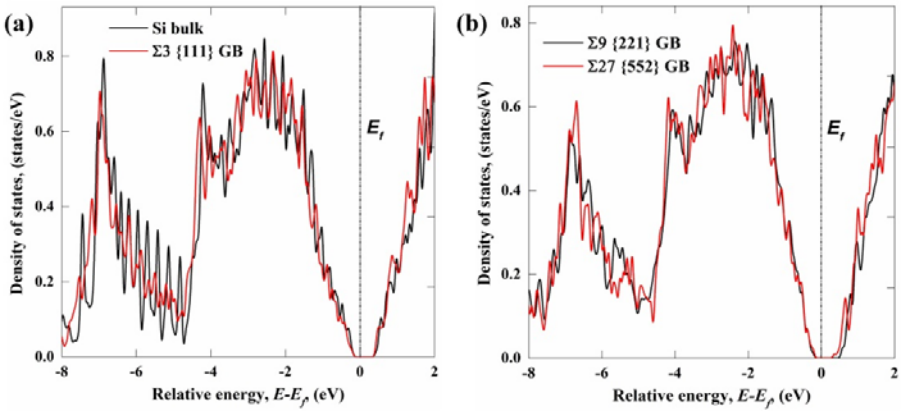

Fig. 5. Total density of states of (a) Si bulk, Σ3 {111}, (b) Σ9 {221} and Σ27 {552} GBs.

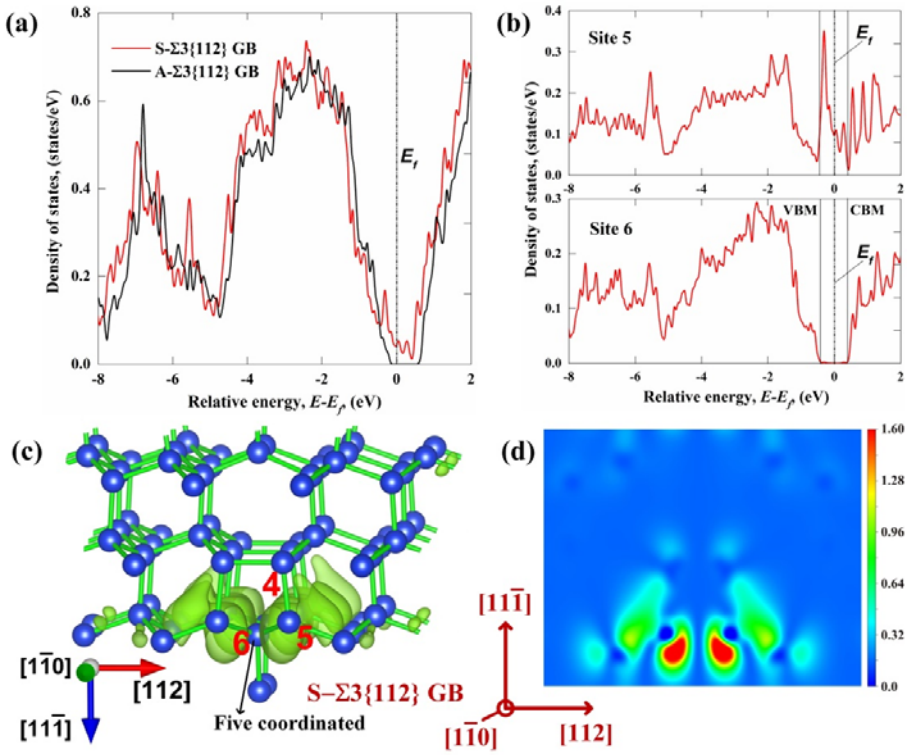

Fig. 6. Total density of states of (a) S- and A-Σ3 {112} GBs with reconstruction along the <1$\bar{1}$0> direction. (b) Partial density of states for Si atoms at core sites 5 and 6 of the (1×2) model of S-Σ3 {112} GB. (c) Charge density isosurface at the density of 1.6×10^{-3} e/Bohr^{-3} for the defect states of S-Σ3 {112} GB in between the CBM and VBM as indicated in Fig. 6b. (d) 2-D charge density contour showing the localized electrons around atomic site 5 which induce the deep levels in the bandgap of density of states of S-Σ3 {112} GB. The unit is 10^{-3} e/Bohr^{-3}.

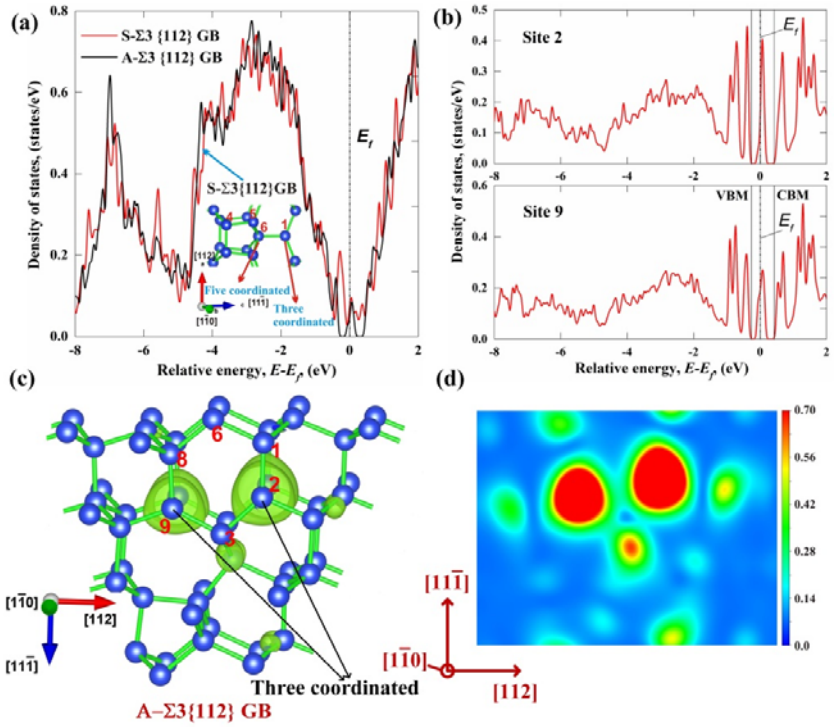

Fig. 7. (a) Total density of states of the CSL (1×1) model of S- and A-Σ3 {112} GBs, which are free of structural reconstruction along the <1$\bar{1}$0> direction. (b) Partial density of states for Si atoms at core sites 2 and 9 of the (1×1) model of A-Σ3 {112} GB. (c) Charge density isosurface at the density of 0.7×10^{-3} e/Bohr^{-3} for the defect states of S-Σ3 {112} GB in between the CBM and VBM as indicated in Fig. 7b. (d) 2-D charge density contour showing the localized electrons around atomic sites 2 and 9 which induce the deep levels in the bandgap of density of states of A-Σ3 {112} GB. The unit is 10^{-3} e/Bohr^{-3}.

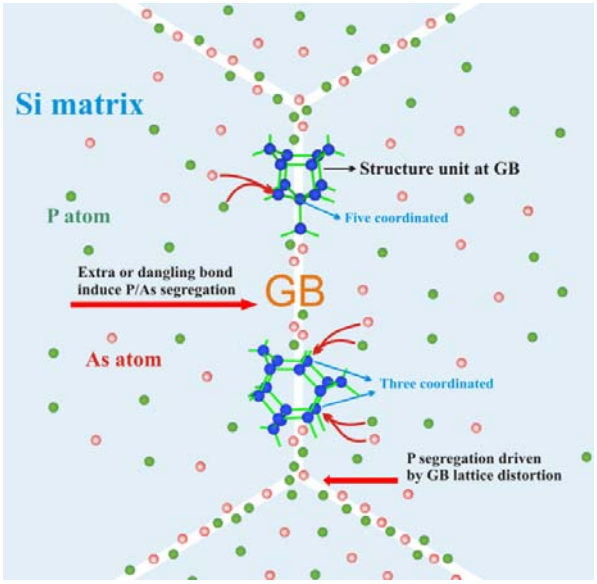

Fig. 8. Schematic for the underlying driving force of P and As segregation at the Si GBs.